^{16}O$(e, e'p)$ results at Q^2=0.8 (GeV/c)^2

J. Ryckebusch* and D. Debruyne
Department of Subatomic and Radiation Physics,
Ghent University, Proeftuinstraat 86, B-9000 Gent, Belgium
(Dated: September 5, 2002)

Fully relativistic calculations employing optical potentials and the Glauber multiple scattering formalism are presented for proton knockout from the p- and s-shell. The role of meson-exchange and Δ-isobar currents is discussed. Two-nucleon knockout contributions to the continuous part of the missing-energy spectrum are computed.

PACS numbers:

I. INTRODUCTION

Popular frameworks to treat FSI effects in modelling $A(e, e'p)$ reactions can roughly be divided in two major classes. At "low" energies ($p_p \leq 1$ GeV/c) most models use optical potentials to determine the scattering wave function for the ejected proton. The parameters in the optical potentials are usually obtained from global fits to elastic $p + A$ scattering data and are available in both relativistic and non-relativistic forms. At higher energies ($p_p \geq 1$ GeV/c), on the other hand, the Glauber model offers good prospects to deal with the distortions which the ejectile undergoes. In the Glauber model, the FSI is calculated directly from the elementary nucleon-nucleon scattering amplitudes $p + N \longrightarrow p + N$. One of the major goals of the work of which some results are presented here, is to provide a framework in which the low and high-energy regime can be bridged. The separation between a "low" and "high-energy" regime in modelling FSI's, is usually done on the basis of the observation that for lab proton momenta p_p exceeding 1 GeV/c the elementary proton-nucleon scattering process becomes highly inelastic.

II. RELATIVISTIC EIKONAL MODEL FOR $\mathbf{A(e, e'p)}$

The fully relativistic model for the description of $A + e \longrightarrow (A-1) + e' + p$ processes which we developed has the following major features [6] [7] [8]. First, it can accommodate relativity in both the description of the electron-proton coupling and the nuclear dynamics. Second, it can be used in conjuction with both the "optical potential" and the "Glauber" framework for dealing with the final-state interactions (FSI). Third, the framework does not use any partial-wave expansion in its numerical computations and can therefore be used to calculate cross sections at high and moderate values of Q^2. Fourth, A$(\vec{e}, e'\vec{p})$ observables can be computed for any target nucleus with $A \geq 4$ provided that its ground-state wave function can be reasonably well described within the context of a relativistic mean-field model. Finally, we provide a completely unfactorized description of the reaction dynamics. This means that our model is **NOT** based on an expression of the type

$$\frac{d^6\sigma}{dT_p d\Omega_p d\epsilon' d\Omega_{\epsilon'}}(e, e'p) = \frac{p_p E_p}{(2\pi)^3}\sigma_{ep} P\left(\vec{p}_m, E_m\right) \ . \qquad (1)$$

The use of this factorized expression was abandoned in the description of low-energy $A(e, e'p)$ process many years ago, but still seems to be common practice when it comes to modeling $A(e, e'p)$ processes at higher energies (for example in calculations addressing proton transparencies). In an unfactorized framework, the $A(\vec{e}, e'p)$ cross section takes on the well-known form in the one-photon exchange approximation

$$\frac{d^5\sigma}{d\Omega_p d\epsilon' d\Omega_{\epsilon'}}(\vec{e}, e'p) = \frac{1}{8\pi^3}\frac{M_p M_{A-1} p_p}{M_A} f_{rec}^{-1}\sigma_{Mott}$$
$$\times\left[v_T W_T + v_L W_L + v_{LT} W_{LT}\cos\phi_p + v_{TT} W_{TT}\cos 2\phi_p + h\left[v'_{LT} W'_{LT} + v'_{TT} W'_{TT}\right]\right] , \qquad (2)$$

where h denotes the electron helicity and the structure functions W depend on the variables (q,ω,p$_p$,θ_p). In the Impulse Approximation (IA) the structure functions W

*jan.ryckebusch@rug.ac.be

are determined by matrix elements of the type

$$m_F^{fi}\left(J^\mu\right) = \langle K_f s_f \left| J^\mu \right| K_i s_i \rangle = \overline{u}_f \Gamma^\mu \left(K_f s_f , K_i s_i\right) u_i \ , \tag{3}$$

where in the final state one has a scattering wave function $u_f(K_f, s_f)$ and in the initial state a bound-state wave function $u_i(K_i, s_i)$. Further, $\Gamma^\mu(K_f\ \ s_f, K_i\ \ s_i)$ represents the off-shell electron-proton coupling. In our model, the *relativistic bound-state wave functions* are obtained within the "$\sigma-\omega$ model" which is a relativistic quantum-field theory for nucleons (ψ) interacting through pions (π's), vector mesons (ρ's and ω's) and scalar mesons (σ's) [5]. The model is usually solved in the Hartree approximation by replacing the scalar and vector meson-field operators by their expectation values.

The determination of the off-shell electron-proton coupling is amongst the weakest parts of any relativistic approach to $A(e,e'p)$ processes ! Indeed, there is some arbitrariness which translates itself in a variety of recipes which all provide identical results for on-shell particles but may lead to substantially different predictions when off-shell nucleons are involved. Amongst the more popular forms for the electron-proton coupling which have been used over the years, we mention

$$\Gamma^\mu_{cc1} = G_M(Q^2)\gamma^\mu - \frac{\kappa}{2M} F_2(Q^2)(K_i^\mu + K_f^\mu) \ , \tag{4}$$

$$\Gamma^\mu_{cc2} = F_1(Q^2)\gamma^\mu + \imath \frac{\kappa}{2M} F_2(Q^2)\sigma^{\mu\nu} q_\nu \ . \tag{5}$$

In determining the scattering wave functions we adopt the relativistic eikonal approximation. This method belongs to the class of semi-classical approximations which are meant to become "exact" in the limit of small de Broglie (db) wavelengths, $\lambda_{db} \ll a$, where a is the typical range of the potential in which the particle is moving. For a particle moving in a typical relativistic (optical) potential, the scattering wave function takes on the following form in the eikonal approximation

$$\psi^{(+)}_{\vec{k},s} \sim \left[\begin{array}{c} 1 \\ \frac{1}{E+M+V_s-V_v} \vec{\sigma} \cdot \vec{p} \end{array} \right] e^{\imath \vec{p}_p \cdot \vec{r}} e^{\imath S(\vec{r})} \chi_{\frac{1}{2} m_s} \ . \tag{6}$$

This wave function differs from a relativistic plane wave in two respects. First, there is a dynamical relativistic effect from the scalar V_s and vector V_v potential, which enhances the contribution from the lower components. Second, the wave function contains an eikonal phase which is determined by integrating the central (V_c) and spin-orbit (V_{so}) parts of the distorting potentials along the escaping particle's (asymptotic) trajectory ($\vec{r} \equiv (\vec{b}, z)$)

$$\begin{aligned} \imath S(\vec{b}, z) &= -\imath \frac{M}{K} \int_{-\infty}^{z} dz' \\ &\quad \times \left[V_c(\vec{b}, z') + V_{so}(\vec{b}, z')[\vec{\sigma} \cdot (\vec{b} \times \vec{K}) - \imath K z'] \right] \end{aligned} \tag{7}$$

where $\vec{K} \equiv \frac{1}{2}\left(\vec{p}_p + \vec{q}\right)$. For proton lab momenta exceeding 1 GeV/c, the use of optical potentials does no longer seem to be fully justifiable in view of the highly inelastic character of the elementary nucleon-nucleon scattering processes. In this energy regime, an alternative description of FSI processes is provided in terms of the Glauber multiple-scattering theory. In such a framework the A-body wave function in the final state reads

$$\psi^{(+)}_{\vec{k},s} \sim \widehat{\mathcal{S}} \left[\begin{array}{c} 1 \\ \frac{1}{E+M} \vec{\sigma} \cdot \vec{p} \end{array} \right] e^{\imath \vec{p}_p \cdot \vec{r}} \chi_{\frac{1}{2} m_s} \Psi_{A-1}^{J_R\, M_R} \left(\vec{r}_2, \vec{r}_3, \ldots \vec{r}_A\right) \ . \tag{8}$$

In this expression, the subsequent elastic or "mildly inelastic" collisions with "frozen" spectator nucleons which the ejectile undergoes, are implemented through the introduction of the following operator

$$\widehat{\mathcal{S}}\left(\vec{r}, \vec{r}_2, \vec{r}_3, \ldots \vec{r}_A\right) \equiv \prod_{j=2}^{A} \left[1 - \Gamma\left(\mid \vec{p}_p \mid, \vec{b} - \vec{b}_j \right) \theta\left(z - z_j\right) \right] \ ,$$

where the profile function for elastic pN scattering reads

$$\Gamma(p_p, \vec{b}) = \frac{\sigma^{tot}_{pN}(1 - i\epsilon_{pN})}{4\pi\beta^2_{pN}}\, exp \left(-\frac{b^2}{2\beta^2_{pN}} \right) \ .$$

In practice, for a given ejectile's lab momentum the following input is required : the total proton-proton and proton-neutron cross sections σ^{tot}_{pN}, the slope parameters β_{pN} and the ratios of the real to imaginary scattering amplitude ϵ_{pN}. We obtain the numbers σ^{tot}_{pN}, β_{pN} and ϵ_{pN} through interpolation of the data base available from the Particle Data Group [1].

III. RESULTS

A. p-shell results

We have compared our relativistic calculations in the eikonal approximation to recent quasi-elastic ^{16}O$(e,e'p)$ data from JLAB. In these high-resolution experiments at $Q^2 = 0.8$ (GeV/c)^2 separated structure functions and polarization transfer data were obtained. In the considered kinematics the de Broglie wavelength of the ejected proton is of the order $\lambda_{db} \approx 0.2$ fm and one may expect the eikonal and Glauber framework to be applicable. At the same time, at these kinetic energies, optical potentials are still readily available.

All numerical calculations use the ^{16}O bound-state wave functions in the parametrization of Ref.'[2], the $CC2$ electron-proton coupling and the Coulomb gauge. Results are displayed for 2 alternative and complementary techniques to compute the effects stemming from the FSI. The adopted techniques are

1. An Optical-Model Eikonal Approximation (OMEA) calculation. Here, the eikonal phase (7) is calculated from the relativistic optical potentials as they are derived from global fits to elastic

proton-nucleus data. We use the energy-dependent atomic-mass independent parametrization for ^{16}O (EDAI-O) version as described in Ref. [9].

2. A Relativistic Multiple-Scattering Glauber Approximation (RMSGA) calculation. In this approach, the scattering state is calculated on the basis of Eq. (8). All parameters entering this calculation are directly obtained from the elementary proton-proton and proton-neutron scattering data.

As can be appreciated from Figs. 1 and 4, the RMSGA and the OMEA approach provide a reasonable description of the cross-section data. A similar remark holds for the separated response functions of Figs. 3 and 6.

Several relativistic calculations based on optical potentials nicely agree with the $1p$-shell $^{16}\mathrm{O}(e,e'p)$ data from E89003 [10, 16]. The novel thing about the results displayed in Figs 1 and 3, is that also an out-of-the box unfactorized and relativistic calculation within the Glauber framework produces fair results.

We have included in our RMSGA and OMEA calculations the contributions from two-body currents stemming from meson-exchange (MEC) and intermediate Δ_{33}-isobar creation (IC). The two-body current contributions to the transition matrix elementes are calculated in the non-relativistic framework outlined in Refs. [14, 15]. The impact of the two-body currents on the computed differential cross sections for p-shell knockout is at the few percent level for low missing momenta and gradually increases with growing missing momentum. Inspecting the response functions of Figs. 3 and 6 the importance of the two-body currents is largest for the R_{LT} response function. It is worth stressing that of all unpolarized response functions, the R_{LT} one is most sensitive to effects beyond the non-relativistic impulse approximation. This feature is well established in deuterium studies [**?**]. It can be understood by considering that in the NRPWIA the transverse amplitude in the R_{LT} response becomes uniquely determined by the convection current. At higher Q^2, the convection current is well established to produce small matrix elements. As a result, the non-relativistic IA contributions, which dominate the R_L and R_T, are suppressed in R_{LT}. This feature makes it an observable which is highly sensitive to any mechanism going beyond the IA, for example relativistic and two-body current mechanisms.

To illustrate the sensitivity of the longitudinal-transverse interference term to MEC and IC, we display in Figs. 2 and 5 the left-right asymmetry

$$A_{LT} = \frac{\sigma(\phi=0^\circ)-\sigma(\phi=180^\circ)}{\sigma(\phi=0^\circ)+\sigma(\phi=180^\circ)} = \frac{v_{LT}R_{LT}}{v_L R_L + v_T R_T + v_{TT} R_{TT}} . \quad (9)$$

The isobar currents are observed to induce bigger effects than the meson-exchange two-body currents.

B. s-shell results

The relativistic IA calculations which provide a nice description of the p-shell data for a missing-momentum range extending up to 400 MeV/c, fail in the s-shell region for missing momenta larger than roughly 100 MeV/c. As can be appreciated from Figs. 7 - 9, the OMEA model (dotted curves), which described the p-shell knockout data reasonably well, also provide a fair description of R_L and R_T for s-shell knockout in parallel kinematics. With increasing θ_{pq} the OMEA model badly underestimates the measured strength when solely one-body current contributions are included.

More than the p-shell responses, the s-shell ones receive sizeable contributions stemming from meson-exchange and intermediate Δ-isobar creation. This can be attributed to the fact that s-shell nucleons are ejected from the high density regions of the nucleus. In these high-density regions, the IA can be expected to be less valid than for proton knockout from more surface dominated single-particle states.

From Figs. 8 and 9 it can be appreciated that the two-body current contributions to single-nucleon knockout from the s-shell, explain a sizeable fraction of the excess R_T and R_{TL} strength. Apart from affecting the single-nucleon knockout cross sections, the two-body currents give rise to multi-nucleon knockout contributions to the continuous part of the missing-energy spectrum. The computed contribution from $^{16}\mathrm{O}(e,e'pp)$ and $^{16}\mathrm{O}(e,e'pn)$ to the continuous part of the missing-energy spectrum is incoherently added to the s-shell knockout strength in Figs.7 - 9. At $\theta_{pq}=0^o$, the two-nucleon knockout contributions is negligible in comparison with the s-shell single-nucleon knockout strength. As the missing momentum increases, the calculated $(e,e'pX)$ accounts for a fair fraction of the measured transverse strength.

IV. CONCLUSION

[1] K. Hagiwara *et al.*, Phys. Rev. D **66** (2002) 01001

[2] C. Horowitz and B. Serot, Nucl. Phys. **A368** (1981) 503.

[3] S. Dieterich *et al.*, Phys. Lett. **B500** (2001) 47.
[4] R. Ransome, contribution to this conference.
[5] B. Serot and J. Walecka, Adv. Nucl. Phys. **16** (1986) 1.
[6] Dimitri Debruyne, Jan Ryckebusch, Wim Van Nespen and Stijn Janssen, Phys. Rev. C **62** (2000) 024611.
[7] D. Debruyne and J. Ryckebusch, Nucl. Phys. **A699** (2002) 65-72.
[8] D. Debruyne, J. Ryckebusch, S. Janssen and T. Van Cauteren, Phys. Lett. **B527** (2002) 62.
[9] E. Cooper, S. Hama, B. Clarck and R. Mercer, Phys. Rev. **C47** (1993) 297.
[10] J. Gao *et al.*, Phys. Rev. Lett. **84** (2000) 3265.
[11] L. Lapikás, G. van der Steenhoven, L. Frankfurt, M. Strikman and M. Zhalov, Phys. Rev. C **61** (2000) 064325.
[12] L. Frankfurt, M. Strikman and M. Zhalov, Phys. Lett. **B503** (2001) 73.
[13] V. Pandharipande, I. Sick and P. deWitt Huberts, Rev. Mod. Phys. **69** (1997) 981.
[14] J. Ryckebusch, D. Debruyne, W. Van Nespen and S. Janssen, Phys. Rev. **C60** (1999) 034604.
[15] J. Ryckebusch, Phys. Rev. C **64** (2001) 044607.
[16] A. Meucci, C. Giusti and F.D. Pacati, Phys. Rev. C **64** (2001) 014604.

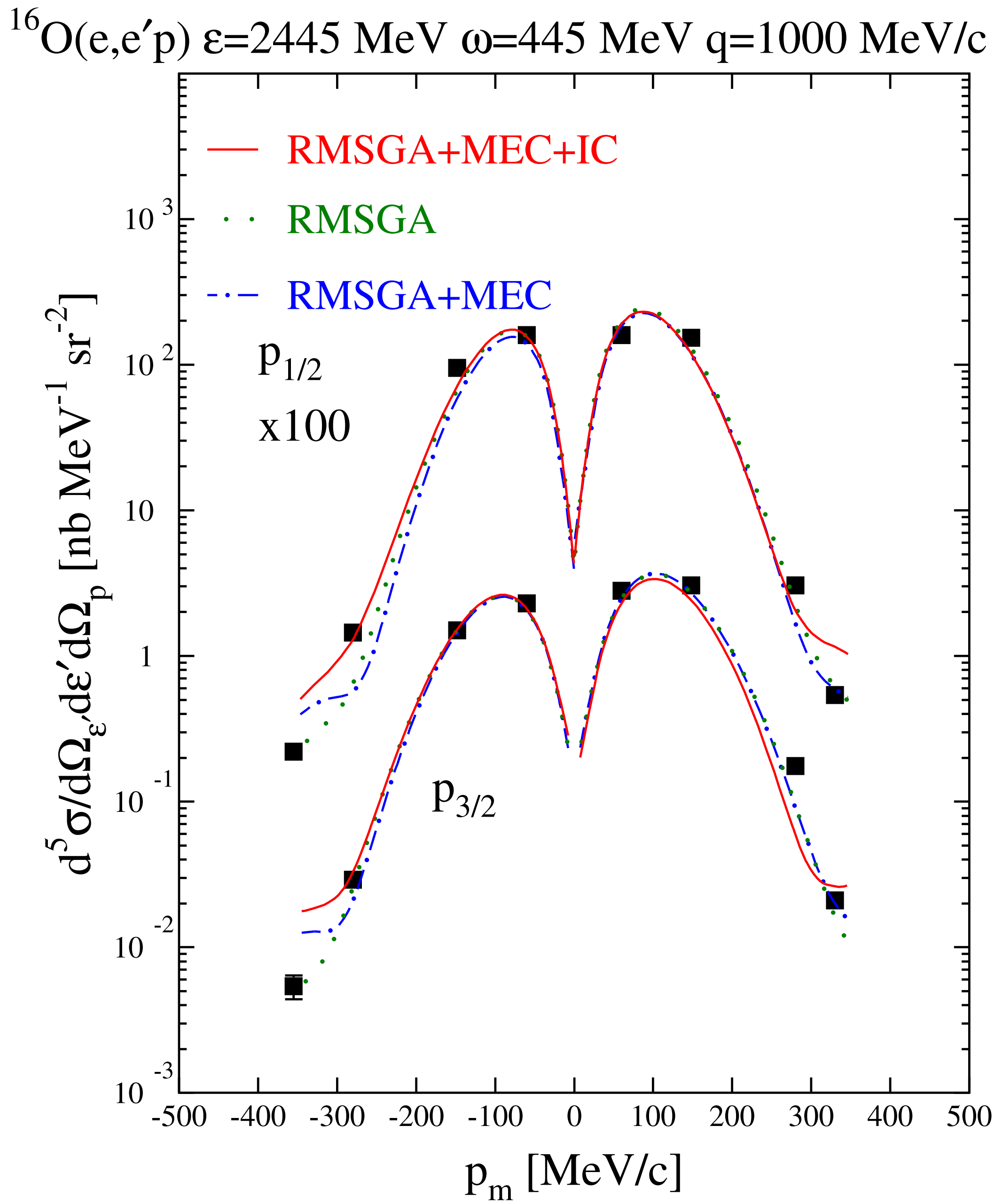

FIG. 1: P_{miss}-dependence of the measured cross sections for the $1p$-shell as compared to Relativistic Multiple Scattering Glauber Approximation (RMSGA) calculations. The dotted line is the relativistic calculation with one-body currents. The dot-dashed line includes also MEC, the solid line MEC and IC. The following spectroscopic factors are adopted $S_{1p3/2}$=0.7 and $S_{1p1/2}$=0.6.

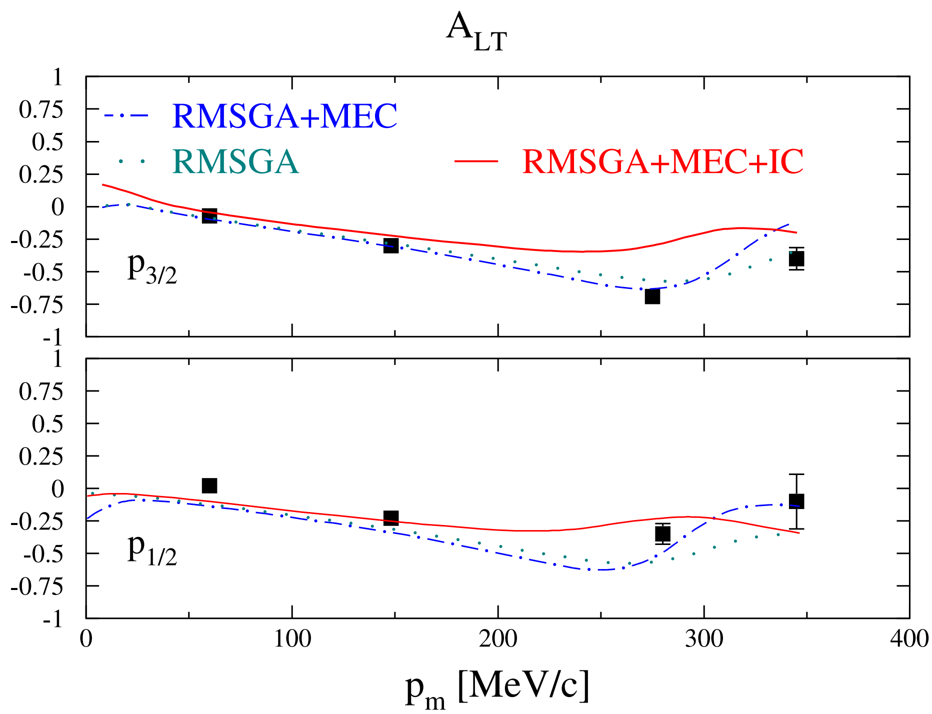

FIG. 2: P_{miss}-dependence of the measured A_{LT} for the 1p-shell as compared to Relativistic Multiple Scattering Glauber Approximation (RMSGA) calculations. The dotted line is the relativistic calculation with one-body currents. The dot-dashed line includes also MEC, the solid line MEC and IC.

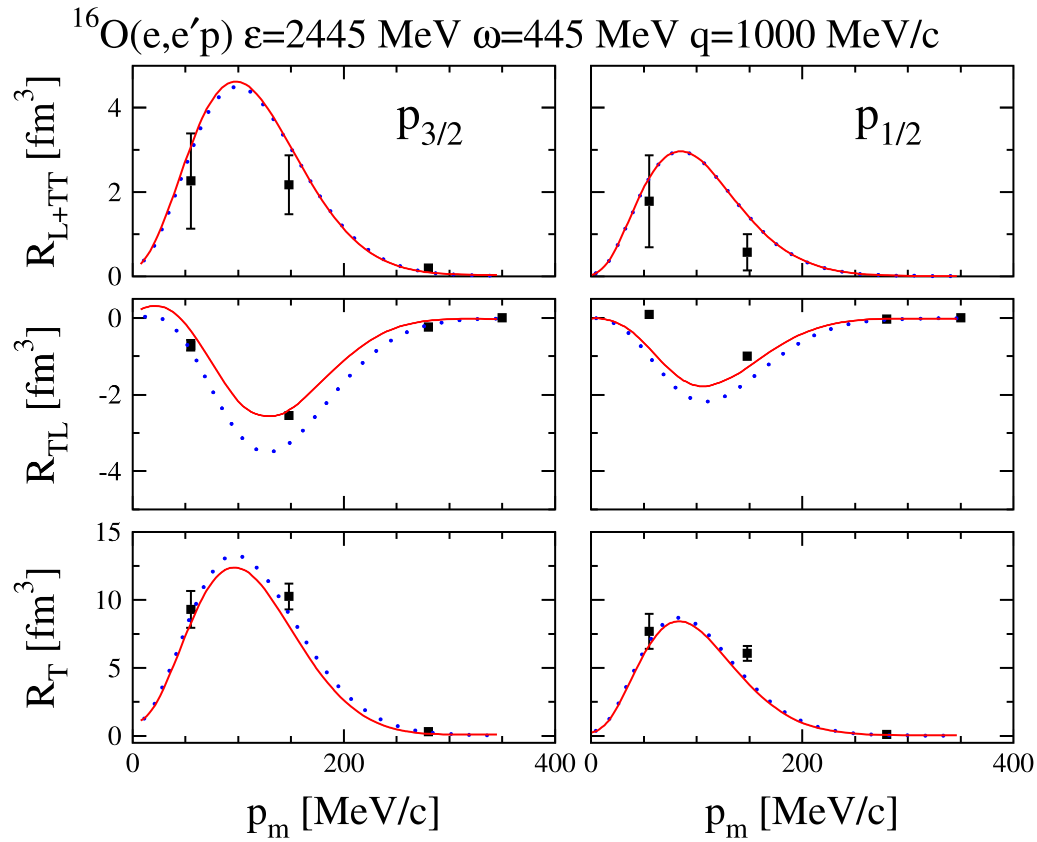

FIG. 3: P_{miss}-dependence of the measured R_T, R_{L+TT} and R_{LT} response functions for the 1p-shell as compared to Relativistic Multiple Scattering Glauber Approximation (RMSGA) calculations. The dotted curve is the fully relativistic calculation with a one-body current. The solid line includes also two-body meson-exchange and isobar currents. The following spectroscopic factors are adopted $S_{1p3/2}$=0.7 and $S_{1p1/2}$=0.6.

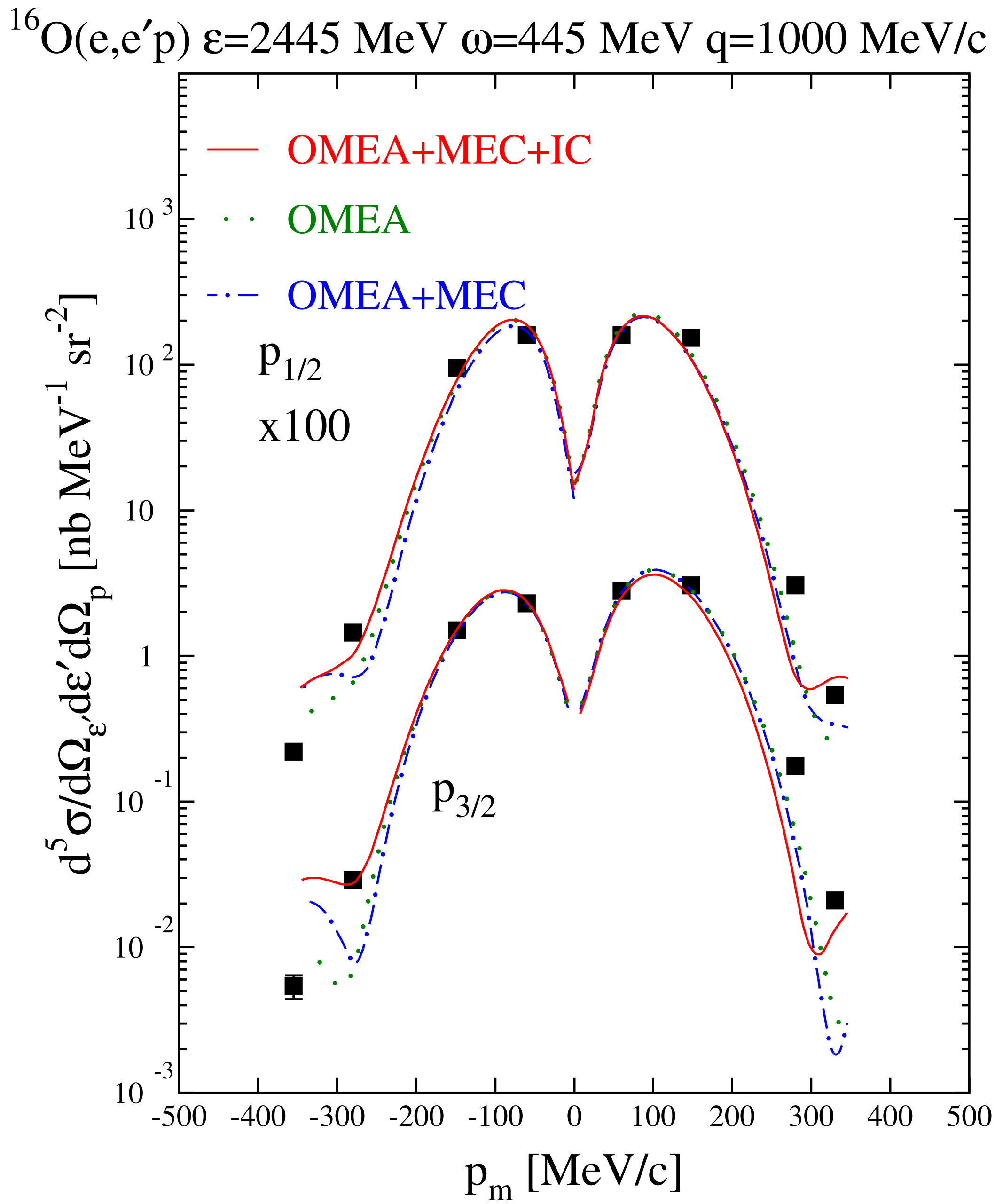

FIG. 4: P_{miss}-dependence of the measured cross sections for the 1p-shell as compared to Relativistic Optical Model Eikonal Approximation (OMEA) calculations. The dotted line is the relativistic calculation with one-body currents. The dot-dashed line includes also MEC, the solid line MEC and IC. The following spectroscopic factors are adopted $S_{1p3/2}$=0.7 and $S_{1p1/2}$=0.6.

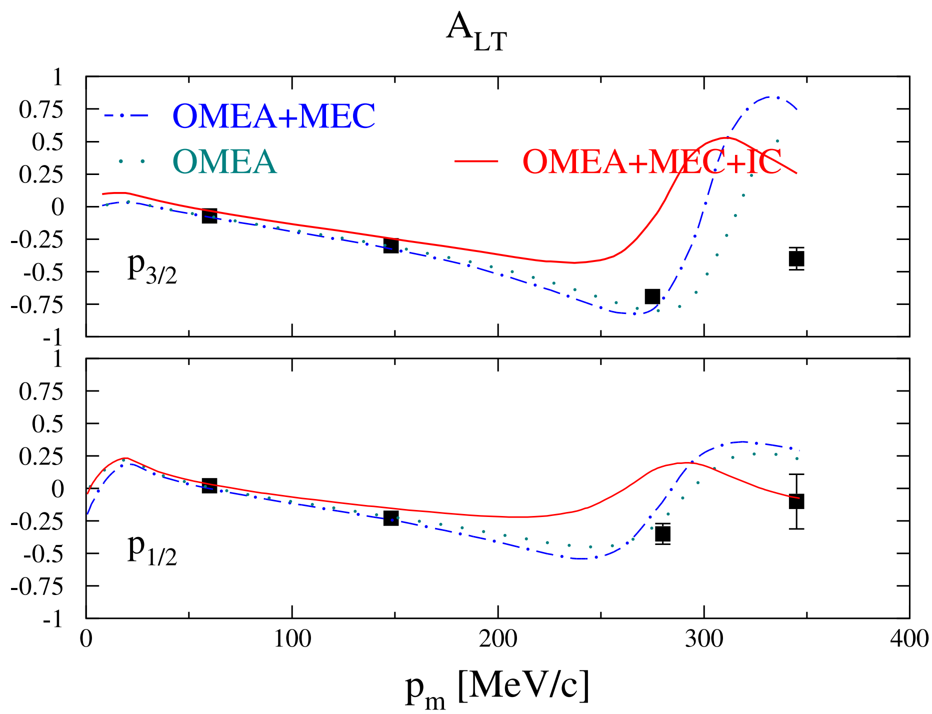

FIG. 5: P_{miss}-dependence of the measured A_{LT} for the 1p-shell as compared to Relativistic OMEA calculations. The dotted line is the relativistic calculation with one-body currents. The dot-dashed line includes also MEC, the solid line MEC and IC.

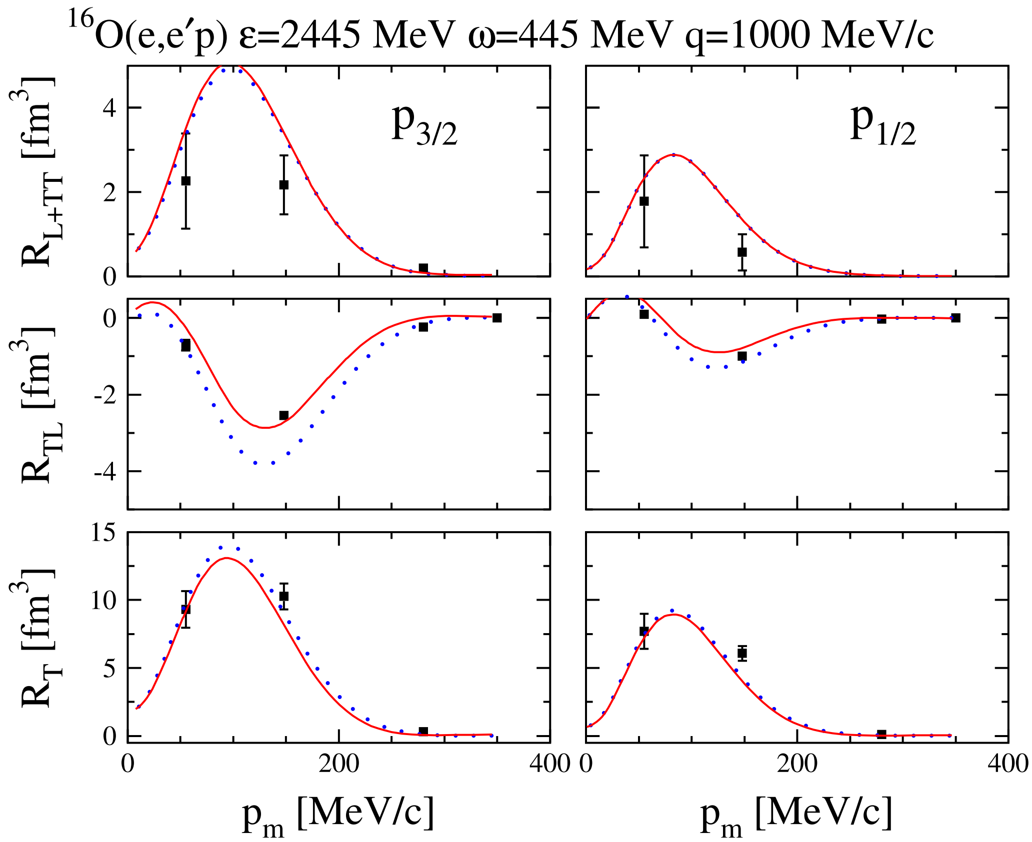

FIG. 6: P_{miss}-dependence of the measured R_T, R_{L+TT} and R_{LT} response functions for the 1p-shell as compared to Relativistic Optical Model Eikonal Approximation (OMEA) calculations. The dotted curve is the fully relativistic calculation with a one-body current. The solid line includes also two-body meson-exchange and isobar currents. The following spectroscopic factors are adopted $S_{1p3/2}$=0.7 and $S_{1p1/2}$=0.6.

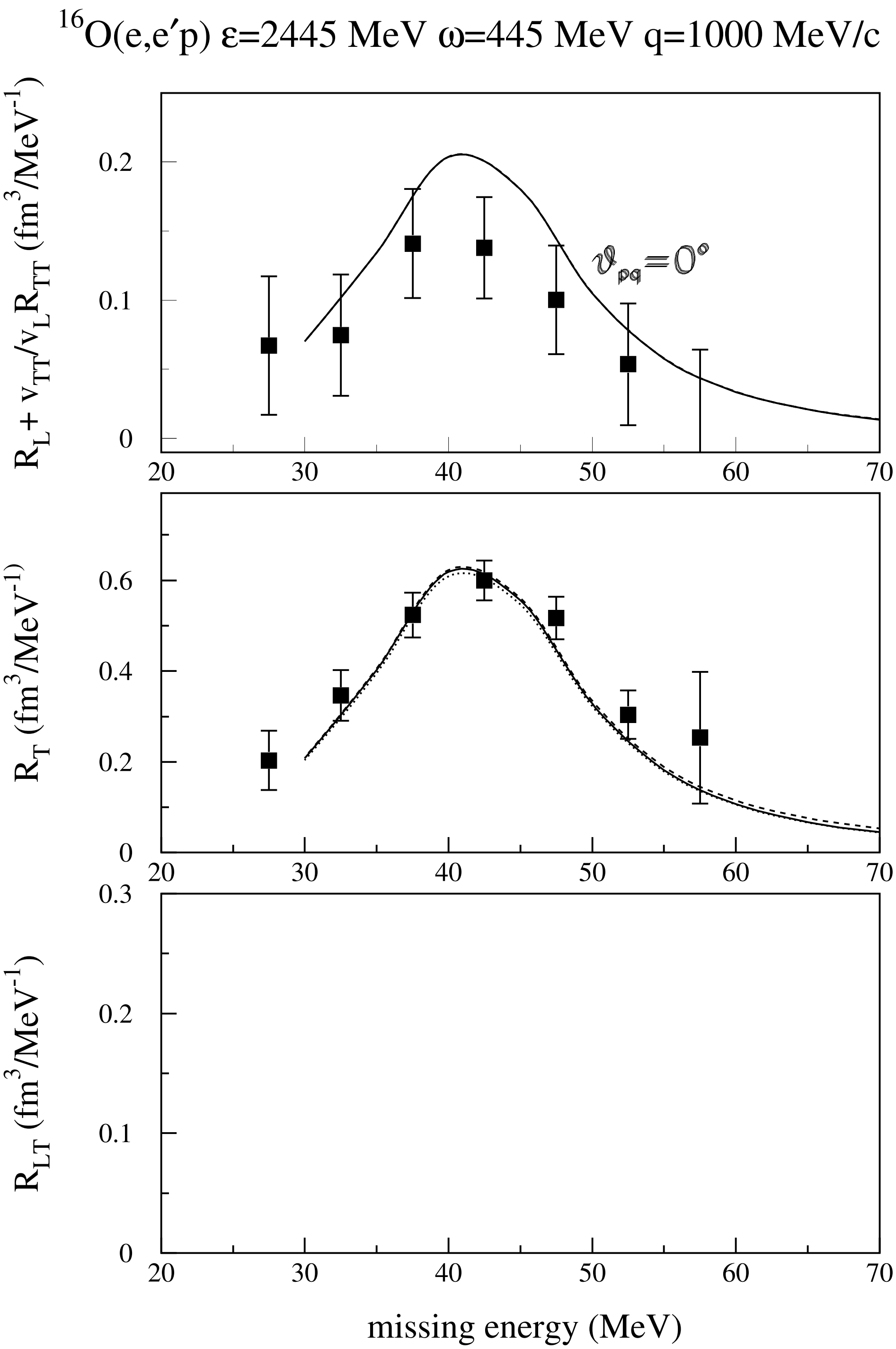

FIG. 7: E_{miss}-dependence of the measured R_T, R_{L+TT} and R_{LT} response functions at $\theta_{pq} = 0^o$ compared to relativistic OMEA and two-nucleon knockout calculations. The dotted curve is the result of a relativistic OMEA calculation for s-shell knockout in the Impulse Approximation. The solid curve includes also the effect of meson-exchange and Δ-isobar currents. The dashed curve is the incoherent sum of the computed ^{16}O$(e, e'pp + pn)$ contribution and s-shell knockout.

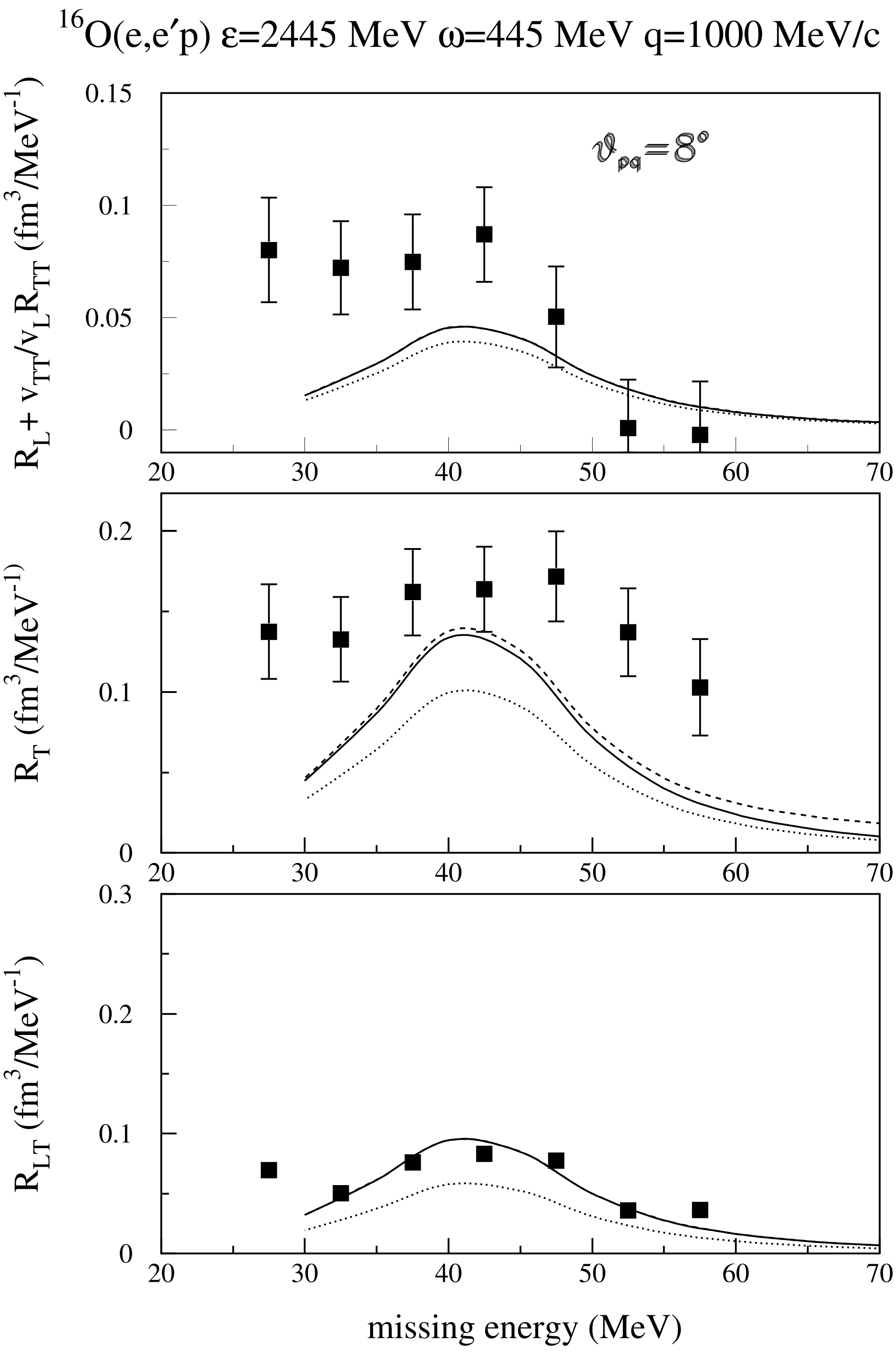

FIG. 8: E_{miss}-dependence of the measured R_T, R_{L+TT} and R_{LT} response functions at $\theta_{pq} = 8^o$ compared to relativistic OMEA and non-relativistic two-nucleon knockout calculations. The dotted curve is the result of a relativistic OMEA calculation for s-shell knockout in the Impulse Approximation. The solid curve includes also the effect of meson-exchange and Δ-isobar currents. The dashed curve is the incoherent sum of the computed $^{16}\mathrm{O}(e, e'pp + pn)$ contribution and s-shell knockout.

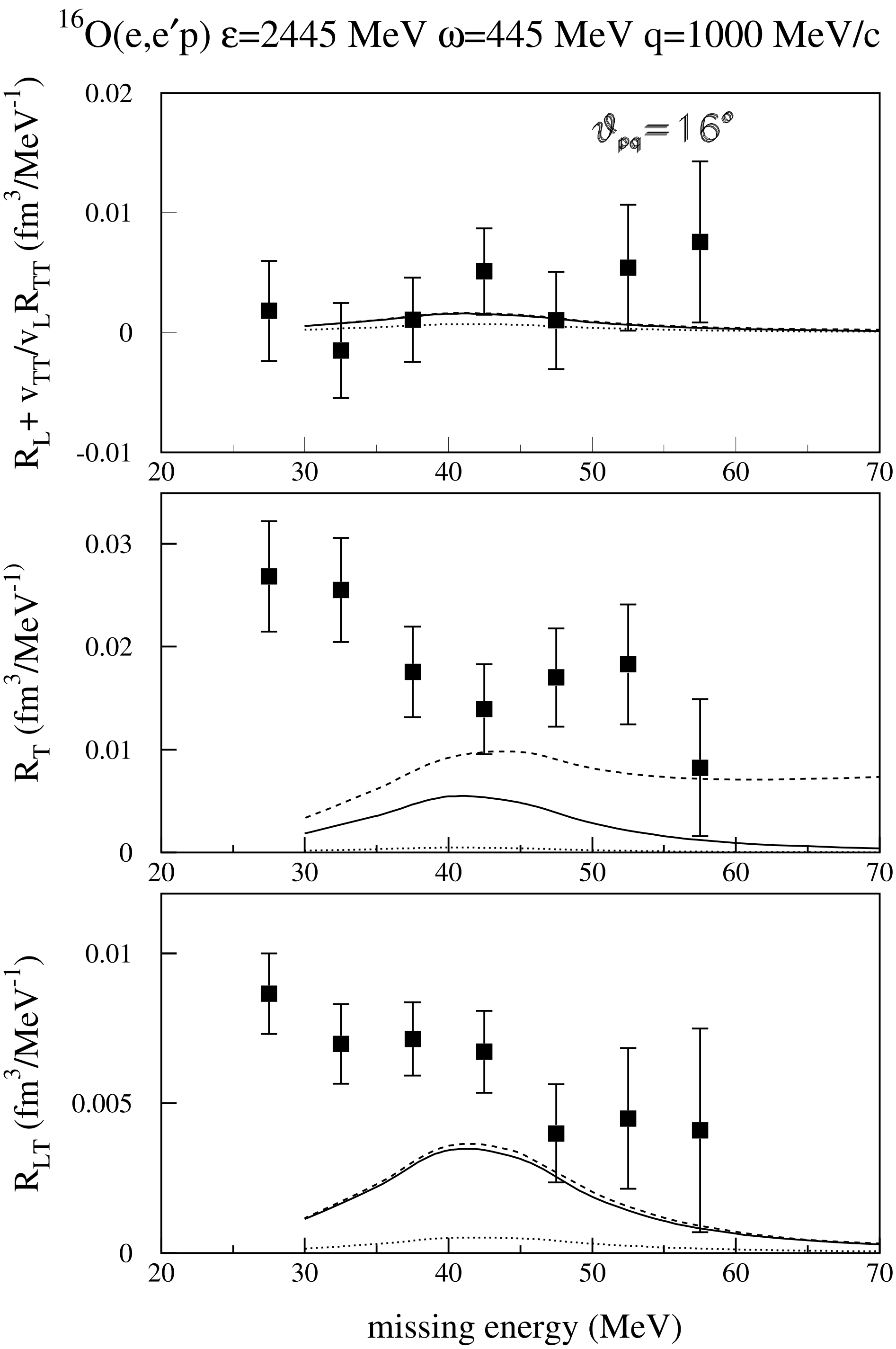

FIG. 9: E_{miss}-dependence of the measured R_T, R_{L+TT} and R_{LT} response functions at $\theta_{pq} = 16^o$ compared to relativistic OMEA and two-nucleon knockout calculations. The dotted curve is the result of a relativistic OMEA calculation for s-shell knockout in the Impulse Approximation. The solid curve includes also the effect of meson-exchange and Δ-isobar currents. The dashed curve is the incoherent sum of the computed $^{16}\mathrm{O}(e, e'pp + pn)$ contribution and s-shell knockout.

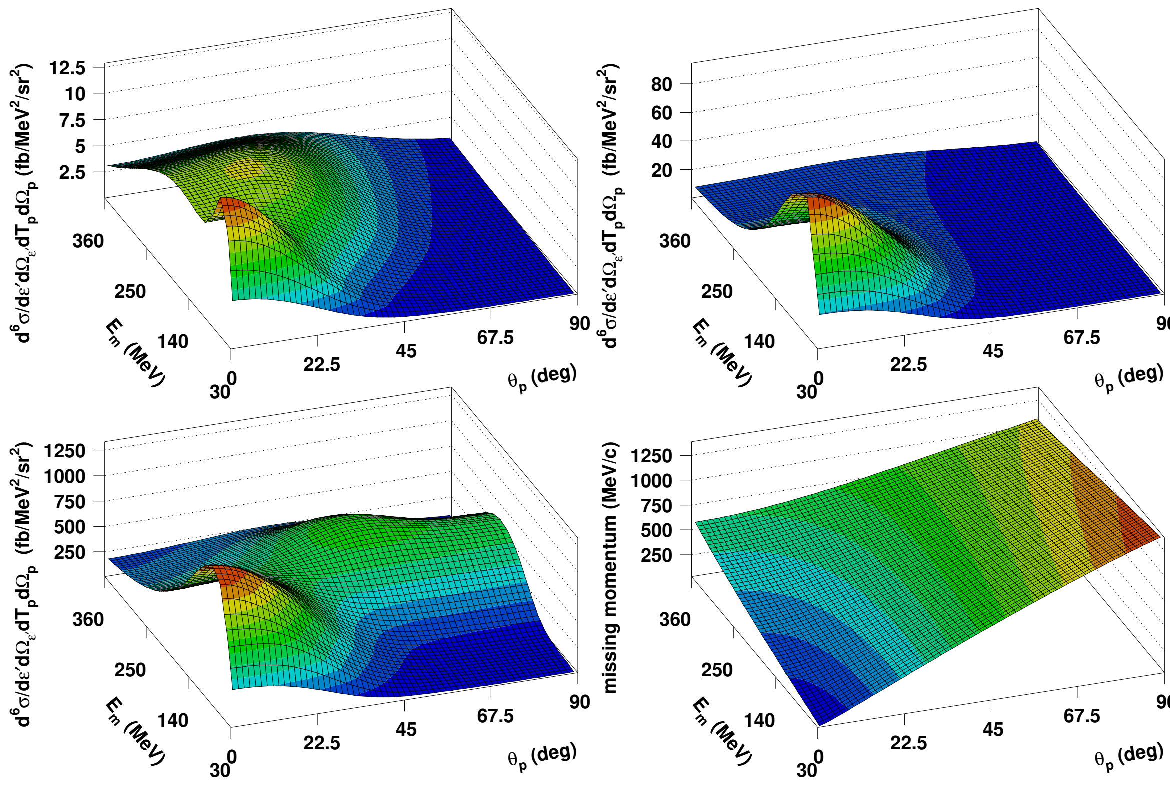

FIG. 10: The calculated contribution from two-nucleon knockout to the differential ^{16}O$(e,e'p)$ cross section versus missing energy and proton angle at ϵ=2.442 GeV, ϵ'=1.997 GeV and θ_e=23.4^o (or, $x \approx 1$ and q = 1.0 GeV/c). The upper left panel includes solely the central correlations and the upper right panel has both central and tensor correlations. The lower left panel, on the other hand, includes apart from the central and tensor correlations also the MEC and IC. The variation of the missing momentum versus missing energy and proton angle is shown in the lower right panel.